Cetineites: Electronic, optical, and conduction properties of nanoporous chalcogenoantimonates

F. Starrost, E. E. Krasovskii, and W. Schattke
Institut für Theoretische Physik und Astrophysik, Christian-Albrechts-Universität Kiel, Leibnizstrasse 15, D-24118 Kiel, Germany

J. Jockel and U. Simon
Institut für Anorganische Chemie, Festkörperchemie, Universität Essen, Schützenbahn 70, D-45127 Essen, Germany

R. Adelung and L. Kipp
Institut für Experimentelle und Angewandte Physik, Christian-Albrechts-Universität Kiel, Leibnizstrasse 19, D-24118 Kiel, Germany
(Received 29 September 1999; revised manuscript received 18 January 2000)

The electronic, optical, and conduction properties of the cetineites, a newly discovered class of crystalline nanoporous materials, have been calculated within a full-potential framework using the augmented Fourier components technique in combination with the extended linear augmented plane-wave $\mathbf{k}\cdot\mathbf{p}$ method. Photoemission, optical, and conductivity measurements have been performed and the calculated results are in conclusive agreement with all available experimental data. This helps in understanding the semiconducting nature of the cetineites, which is an exceptional property for nanoporous crystals.

I. INTRODUCTION

Cetineites are crystalline nanoporous chalcogenoantimonates that have been discovered only recently.[1] The crystals are formed by tubes of subnanometer diameter arranged in a hexagonal rod packing. In contrast to the structurally related and well-known zeolites, the traditional molecular sieve materials, and heterogeneous catalysts[2] that are electrical insulators, the cetineites have a semiconducting host lattice. This property is so far unique in the domain of nanoporous crystalline solids. Thus, new possibilities are opened, ranging from nanosensors to electrically switched molecular sieves. The long, regularly arranged tubes with a diameter of about 0.7 nm suggest applications as chemical sensors or microlasers, arising from the deposition of molecules or nanoparticles inside the channels.[3,4] Therefore, the chemical synthesis of the cetineites can be viewed as an example for the bottom-up design of nanostructures. In this approach, rather than construct the miniature electronic circuits through complex physical processes on substrates, the devices are to be grown in the chemist's tube.[3,5–7]

Progress has been made in the chemical synthesis of large cetineite single crystals.[8,9] Up to now a large number of crystals with different composition have been obtained by hydrothermal synthesis. Further investigations are under way for the chemical control of the desired properties, e.g., tailoring the band gap and other semiconductor properties.[10]

First *ab initio* calculations of the cetineite electronic structure[11,12] already have shown remarkable agreement with experimental findings. The newly developed augmented Fourier component (AFC) method,[13] however, gives us the possibility to improve upon the earlier calculations by treating the crystal potential more realistically than by the muffin-tin approximation used before. In our earlier calculations, computational necessity demanded that corrections to the flat interstitial part of the potential were only applied through the introduction of spheres empty of charge in the open channels that may have distorted the actual charge distribution. The AFC extended linear augmented plane-wave (ELAPW) $\mathbf{k}\cdot\mathbf{p}$ method now offers a possibility to determine self-consistent general-shape potentials with high accuracy in a reasonable time frame. For the calculation of the optical and conduction properties, which require the computation of energies and wave functions for a large number of $\mathbf{k}$ points, the perturbational $\mathbf{k}\cdot\mathbf{p}$ method is used.

In this paper we intend to explore the electronic, optical, and conduction properties of the cetineites. Theoretical advances as well as further experimental achievements provide a conclusive insight into structure/property relations. In Sec. II the history and chemical synthesis of the cetineites is presented. Section III gives an introduction to the AFC method and lists the computational details. The experimental results, obtained in the way described in Sec. IV, are compared with the calculated properties in Sec. V.

II. CETINEITE STRUCTURE

The cetineite mineral was first described in 1987 by Sabelli and Vezzalini,[1] who found crystals of it in Le Cetine mine in Tuscany, Italy, a place famous among mineral collectors. Early in the twentieth century the mine had been used to extract antimony from stibnite (Sb_2S_3) ore. Slags from the extraction process were deposited on heaps where—among a number of other minerals—cetineite crystals formed in cavities as a result of the natural weathering of the residuals of the mining process.

The cetineite crystals found at the mine have the formula $(K,Na)_{3+x}(Sb_2O_3)_3(SbS_3)(OH)\cdot(2.8-x)H_2O$ with $x \approx 0.5$.[14] They occur as tufts of acicular (needlelike) crystals where the needles are parallel to [0001]. The orange-red crystals have been found with lengths up to 0.5 mm and 15 μm in diameter. A photograph is shown in Fig. 1.

A number of synthetic analogs of the cetineite mineral are known. The general formula is $A_6[Sb_{12}O_{18}][SbX_3]_2\cdot(6-mx-y)H_2O\cdot x[B^{m+}(OH^-)_m]\cdot y\square$, where $A=Na^+$, K^+, Rb^+; $X=S^{2-}$, Se^{2-}; $B=Na^+$, Sb^{3+}; and $\square$ may stand for

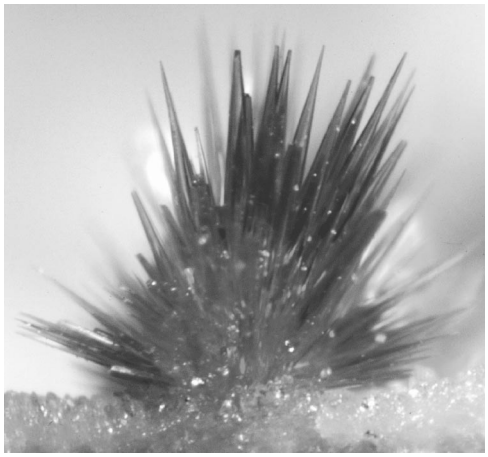

FIG. 1. A photograph of a cetineite mineral (copyright by Robert Vernet, Collection G. Favreau, used by kind permission).

an unoccupied lattice site. The crystal formulas are abbreviated by $(A;X)$.

Even before the natural mineral was found, Graf and Schäfer described a synthetic analog of (K;S) in 1975.[15] The diffraction data, however, did not reveal the presence of the channel-filling guests. Since then several analogs have been synthesized (and their structure has been described) by Nakai *et al.* and Kluger and Pertlik (see Ref. 14), Wang and Liebau,[16–18] Jockel,[19] and Simon *et al.*[8] Progress in the synthetic method yields the preparation of single crystals up to a length of 2 mm and a hexagonal cross section of 3×10^{-2} mm^2.[9] In the following the synthetic analog crystals will be referred to as ''cetineites.''

The two main structural characteristics of cetineite crystals are large infinite $Sb_{12}O_{18}$ tubes and isolated SbX_3 pyramids (see Figs. 2 and 3). A tube is made of interconnected SbO_3 pyramids and has a 6_3 axis. The tubes form a two-dimensional hexagonal lattice perpendicular to their axes as is found in ordered arrangements in single-walled carbon nanotubes.[20] The SbX_3 pyramids are located in the tubular interstices; the plane in which the three X atoms lie is perpendicular to the tube axes. In a single interstice, infinite in the c direction, all pyramids have the same orientation; this orientation, however, varies at random from one interstice to the next. When all interstitial pyramids point in the same direction the crystal space group is $P6_3$. The tube arrangement without the interstitial pyramids has an additional symmetry, a mirror plane perpendicular to the axis in the plane containing the O(1) and the A atom, i.e., the space group $P6_3/m$. The hexagonal lattice constants for the cetineite class are 1.41 nm$\lesssim a\lesssim$1.46 nm and $c\approx0.55$ nm; the voids within the tubes have a diameter of approx. 0.7 nm.

From chemical considerations it is assumed that there are strong Sb—O bonds that stabilize the $Sb_{12}O_{18}$ tubes. The binding among the tubes is thought to be via the SbX_3 pyramids, which are assumed to have ionic bonds to the A atoms on the internal wall of the tube[15] and additional weaker bonds to the Sb(2) atoms of the tube wall (numbers in parentheses following the atom name denote geometrically inequivalent atoms of the same species.)

The host lattice can—and easily does—accept a number of guest molecules. A common guest species is water in connection with the B^{m+} molecules, where B is an alkali

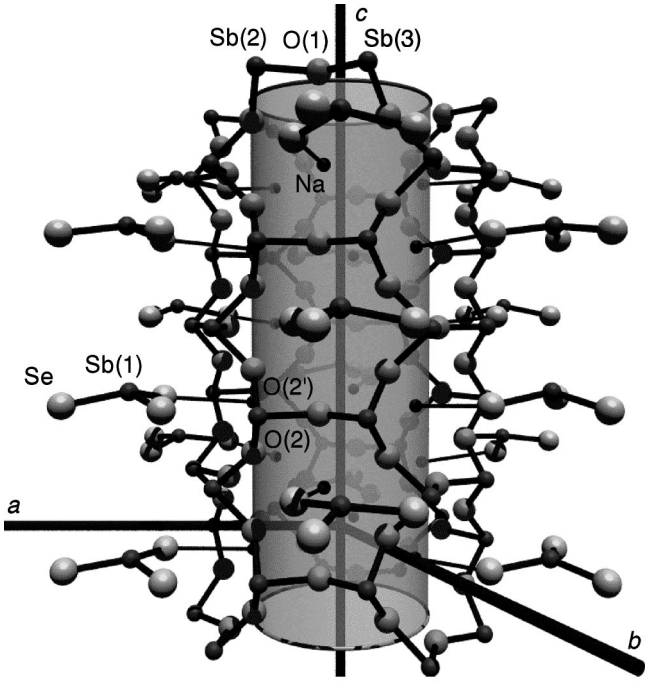

FIG. 2. A perspective view of the cetineite (Na;Se). The shaded tube is included only as a guide for the eye.

metal, for example. Water molecules can be extracted from the tubes by evacuating the environment and heating the crystals. However, the ease of extraction and the degree to which it is actually performed is dependent on the specific crystal. Defects in the tubes hinder the extraction. Simon *et al.*[8] report that from well-formed crystals of (K;Se) the water can be expelled at room temperature in high vacuum within a few seconds.

III. THE AUGMENTED FOURIER COMPONENT METHOD: COMPUTATIONAL DETAILS

Linear augmented plane-wave (LAPW) calculations yield the electronic band structure and wave functions of a very high accuracy.[21] The muffin-tin approach to the crystal density and potential, which adopts spherical averaging of these

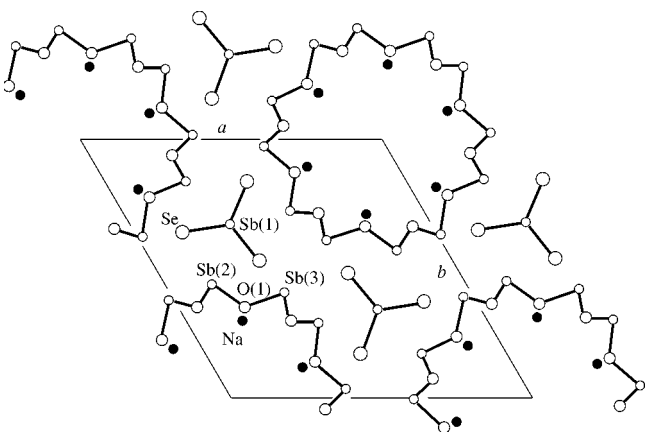

FIG. 3. The cetineite (Na;Se) viewed from the top.

two functions in the muffin-tin spheres around the atoms and constant quantities in the interstitial region, yields very good results for close-packed materials, such as elementary metals.[22] However, in open structures, where the interstitial region has a volume equal to or greater than the volume covered by the muffin-tin (MT) spheres, the approximation is hard to justify. In the semiconductor silicon, for example, which crystallizes in the diamond structure where only 34% of the unit cell volume is covered by touching MT spheres, the muffin-tin approximation will not yield a band gap in the electronic band structure. A first step to remedy this situation is the introduction of ''empty spheres,'' additional spheres without any atomic nuclei where the charge density and the potential are allowed to take on values different from the rest of the interstitial volume, thus adding a primitive corrugation of the functions there. A better solution is a potential that can take on a general shape, as is implemented in the well-known full-potential LAPW (FLAPW) method.[23]

The FLAPW method has shortcomings, however, particularly in its convergence properties, which is the reason why we have developed the augmented Fourier component (AFC) method.[13] The main difference between the two methods is that while in the FLAPW method the APW representation is retained for the construction of the charge density, in the AFC method the density is separated into two parts: a Fourier part, $\rho^F(\mathbf{r})$, which represents the charge density of the valence electrons, and a narrow MT part, $\rho^{MT}(\mathbf{r})$, describing the nucleus and the core electron distribution in a spherically symmetric average. The Fourier charge density distribution is easily accessible in this method because the ELAPW $\mathbf{k}\cdot\mathbf{p}$ method easily yields the Fourier transform of the valence wave functions. Additionally, the AFC method can be accelerated by transferring charge, whose distribution is given by the higher Fourier components of ρ^F, to the MT part. This combination of a significant gain of speed and a tiny and controllable loss of accuracy makes possible very quick LAPW calculations with a general-shape potential. The extension of the ELAPW AFC method to structure optimization is straightforward; however, this feature still is to be implemented in the computer code.

The perturbational $\mathbf{k}\cdot\mathbf{p}$ method is a traditional $\mathbf{k}\cdot\mathbf{p}$ approach in which the lower 1000 solutions at the reference point $\mathbf{k}_0$ multiplied by a phase factor $\exp[i(\mathbf{k}-\mathbf{k}_0)\cdot\mathbf{r}]$ are used as basis functions. Using this approach we significantly reduce the size of the Hamiltonian matrix and the overlap matrix is the unity matrix. Since the AFC method provides the Fourier transform of the wave functions and the momentum operator is diagonal in a plane-wave basis the calculation of the momentum matrix elements is simplified and the order of scaling in the construction of the Hamiltonian matrix is reduced. This approach has generally been used for calculations requiring a larger number of $\mathbf{k}$ points.

For the calculations a simplified structure of that given in Sec. II has been used: The contents of the inner tubes have been dropped so that the formula is $A_6[Sb_{12}O_{18}]\ [SbX_3]_2$. Also, the orientation of the intertubular pyramid chains has been assumed to be parallel in all cases. For (K;Se) the $2\times2\times1$ superstructure has not been taken into account. The unit cell contains 44 atoms of 8 inequivalent types with the atomic positions and lattice constants taken from x-ray diffraction data.[7] These experimental parameters have been established to a high degree of confidence. Calculations with slightly differing positions from earlier experiments (concerning mainly the position of the chalcogen) showed that the main features of these results are stable with respect to small changes of the geometry. The guest ions B^{m+} and the water molecules or hydroxyl groups OH^- have been left out of the calculations because they are considered to be strongly disordered[24] and the presented discussion neither needs nor justifies the additional computational burden at this stage. An ionic conductivity, however, carried by the water and/or the B^{m+} ions has been excluded through impedance measurements.[8] The lattice constants are given in Table I.

TABLE I. The lattice constants used for the calculations of the four cetineites (in nm).

	(K;Se)	(Na;Se)	(K;S)	(Na;S)
a	1.4630	1.4423	1.4318	1.4152
c	0.5616	0.5565	0.5633	0.5576

All the results presented here were calculated using the AFC ELAPW $\mathbf{k}\cdot\mathbf{p}$ method. The calculation of all observables is based on self-consistent potentials determined by the AFC method. The basis size of the decisive calculations was 3000 functions, or about 70 APW's per atom. This ratio has been found to be sufficient for other complex structures, such as perovskites.[25] For Ru_2Si_3, Wolf *et al.* find that the electronic structure is well converged with 75 LAPW's per atom.[26] The parameter $|\mathbf{G}_{max}|S_{min}$ was about 4.5, where S_{min} is the smallest sphere radius. For the self-consistent calculations, the densities were computed at the $\mathbf{k}$ point Γ, which is justified by the large real-space dimensions of the unit cell translating into a very small Brillouin zone.

Earlier calculations[11,12] were carried out within the muffin-tin approximation. Aspherical corrections were introduced by adding an empty sphere within the tubes. The new results using the AFC method presented here offer a much better description of the physics. The results show that the former calculations describe the basic properties of the cetineites; however, new and important effects are discovered by this highly accurate calculation.

IV. EXPERIMENTAL SETUPS

Three experimental methods were used to determine the crystals' band gaps: (1) transmission spectroscopy using ultraviolet/visual light (UV/vis),[8] (2) wavelength-dependent measurement of the photoconductivity,[19] and (3) measurement of the thermal activation energy.[9,27]

All measurements have been performed under ambient conditions on individual single crystals of each cetineite phase, which have been synthesized under hydrothermal reaction of elementary antimony and sulfur or selenium, respectively, in aqueous NaOH or KOH.[9] Since the $a\times b$ faces of the crystals in some cases have shown to be capped by an amorphous oxide layer the crystals' ends have been broken off. Conductivity measurements have been performed by providing silver contacts to the clean faces as well as to the sides (see Fig. 11). Besides (K;Se), where the tubes are just occupied by removable water molecules, all other compounds show traces of Sb^{3+}, Na^+, or K^+ ions, in addition to

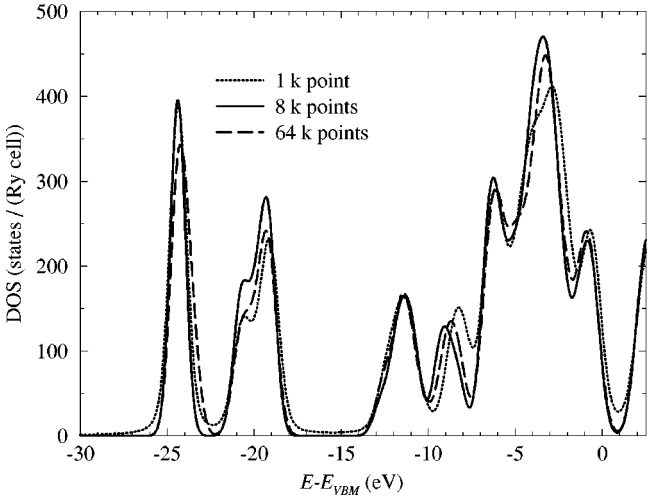

FIG. 4. The density of states of the cetineite (Na;Se) computed by three different methods: with a single **k** point and 8 **k** points using the AFC ELAPW **k**·**p** method and with 64 **k** points using the perturbational AFC ELAPW **k**·**p** method. The curves have been convoluted with Gaussian curves of a full width at half maximum (FWHM) of 1 eV.

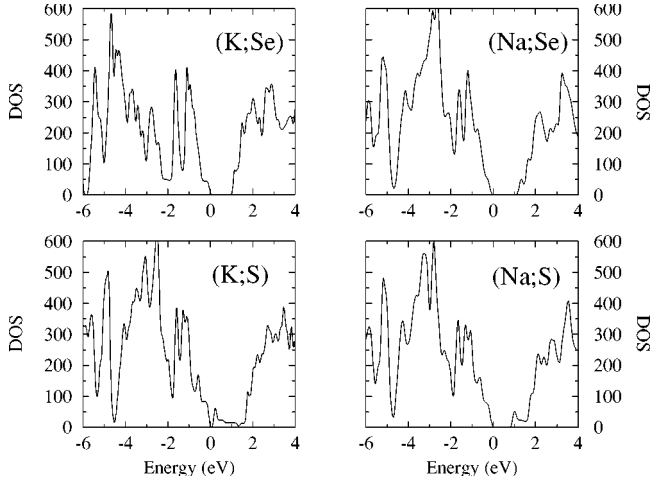

FIG. 5. The DOS for the four cetineites (K;Se), (Na;Se), (K;S), and (Na;S) for the valence region. It has been calculated with the perturbational **k**·**p** method for 64 **k** points in the IBZ. The (Na;Se) DOS shown in Fig. 4 is the one displayed here convoluted with a Gaussian.

water and OH^-. These ions could not be extracted, presumably due to structural defects.

Using the first two methods, band gaps in the region of about 2.0–2.4 eV were observed, whereas the temperature-dependent measurements yielded activation energies of about 0.5 eV reflecting a fundamental gap of about 1.0 eV. Photoemission spectroscopy experiments have been done on samples of a number of randomly oriented crystals with a photon energy of 21.22 eV from a helium Iα discharge lamp. The overall energy resolution was chosen to be better than 100 meV. Random orientation was viewed as an angle integration to compare the photocurrent with the calculated density of states.

V. RESULTS

For the four cetineites (K;Se), (Na;Se), (K;S), and (Na;S) a number of electronic and optical properties have been calculated, which here will be compared to the experimental results where available.

A. The density of states

To show that our approach is viable the density of states (DOS) of the compound (Na;Se) has been computed in three different ways all based on the AFC ELAPW **k**·**p** method (see Fig. 4). One of the two curves calculated with the exact ELAPW **k**·**p** method is the sum of Lorentzians centered at Γ point band energies, while the other is derived from a calculation with 8 **k** points in the irreducible part of the Brillouin zone (IBZ). The third curve was derived using the perturbational **k**·**p** method for 64 **k** vectors (the IBZ has 1/12th the volume of the full Brillouin zone). The comparison in Fig. 4 shows that all three methods give the same result to a very high degree. This does not only mean that the single-**k**-point method is justified but also that the perturbational **k**·**p** method describes the electronic structure of the valence band region with very small differences from the exact **k**·**p** method. Shifts in the peaks of the three DOS curves due to the dispersion of the band structure are minor. The worst example is the peak at about -9 eV, which in the single-**k**-point approximation is shifted by about 0.5 eV to higher energies.

In all four of the cetineites, the valence DOS has one major band ranging from the Fermi energy to about -6 eV. This peak can be roughly subdivided into two manifolds, ranging approximately from 0 to -4 eV and from -4 to -6 eV. To a large degree the states in the first manifold are hybridized O $2p$ and chalcogen p states, where the chalcogen p character dominates near the highest occupied state. The lower energy manifold is almost exclusively made up of oxygen p with a small contribution from Sb p. The states in the energy interval from -6 to -8 eV are mainly of Sb $5s$ and O $2p$ character. So the binding of O and Sb in the wall is carried out by the states in these two energy intervals. The lower unoccupied states are to a large degree hybridized p orbitals of all the atoms in the crystal, except for the alkali metal. In the cetineites containing sulfur at **k** point Γ, the lowest unoccupied state is strongly delocalized in the c direction and is confined entirely to the interior of the Sb_2O_3 channels. Similar nearly-free-electron-like states have been observed in calculations on boron nitride nanotubes.[28] It will be difficult to experimentally observe this state in samples whose tubes are not completely evacuated since we expect it to be destroyed by impurities. In the following discussions of gap sizes this state is therefore treated separately.

The densities of states for the four substances show a gap of between 1.5 and 1.8 eV (see Fig. 5). In the crystals containing sulfur, (K;S) and (Na;S), within this gap the DOS of the single free-electron-like state mentioned above appears, which narrows the gap to 0.1 and 1.0 eV, respectively. This single state has a very high dispersion. These states are also visible, with some distortions indicating hybridization, at higher energies among the conduction bands of the selenium compounds. In the energetic interval extending a few electron volts around the gap this band is easily identified and it

TABLE II. Optical gaps of the cetineites. The size of the gaps of the cetineites determined by measuring the absorption threshold $E_{gap-trans}$, the onset energy of the photoconductivity $E_{gap-photo}$ and calculating the first maximum of the squared plasma frequency $E_{gap-theor}$ as well as the indirect band gap $E_{indirect}$ taken from the band structure neglecting the gap state.

Crystal	(K;Se)	(Na;Se)	(K;S)	(Na;S)
$E_{gap-trans}$	2.03 eV	2.12 eV	2.29 eV	2.38 eV
$E_{gap-photo}$	2.10 eV	2.15 eV	2.25 eV	2.40 eV
$E_{gap-theor}$	2.2 eV	2.4 eV	2.5 eV	2.6 eV
$E_{indirect}$	1.0 eV	1.3 eV	1.6 eV	1.7 eV

is an obvious feature to display significant changes from one compound to the next, whereas the other bands appear largely unchanged.

The earlier calculations using the muffin-tin approximation of the potential yielded fundamental gaps of about 0.5 eV.[11,12] The muffin-tin potential approximation leads to a narrowing of the gap, an effect that also appears in the semiconductor silicon, for example, where the self-consistent muffin-tin potential yields a semimetal.[29] The gap size calculated by the AFC method still is slightly too small, which appears to be an effect of the treatment of many-particle interactions in the local density approximation (LDA).

Using photoconductivity measurements and uv/visible spectroscopy a gap size of slightly above 2 eV was obtained at room temperature. The values are given in Table II.

By scanning through the temperature and monitoring the conductivity the electronic activation energies have been found, i.e., the minimum thermal energies that are necessary to excite electrons from the Fermi edge into the conduction band so that significant conductivity can be registered. For the (Na;Se) crystals the temperature interval was from 326.5 to 238.5 K and an activation energy of 0.43 eV was found. Going from 294 to 229 K the activation energy in (K;Se) was 0.48 eV, from 240 to 310 K in (K;S) yielded 0.5 eV and from 268 to 327 K in (Na;S) yielded 0.55 eV. This must be compared with 1/2 the values of the indirect gaps of the band structure (see Table II).

The calculated density of states is compared to an angle-integrated photoemission spectrum of (Na;Se) taken at 21.22 eV photon energy. In Fig. 6 one can see that the oxygen $2p$–derived peak at about -3 eV and the antimony $5s$–derived peak at about -12 eV are reproduced. Their relative intensities agree with those suggested by the DOS curve. Two structures in the DOS at -6 and -9 eV are not resolved. That may possibly be due to the selection rules of the photoemission process, which have not been taken into account here or may be because only an incomplete angle integration has been achieved on the experimental side by averaging the emissions from a number of differently oriented crystals.

B. The band structure

The band structure of the (Na;Se) compound is shown in Fig. 7. The cetineite band structures have a very similar structure, where corresponding bands can easily be identified even though they sometimes are shifted energetically with respect to each other. The most striking feature of cetineite band structures is the stronger dispersion along the c axis, i.e., in the ΓA direction. This dispersion indicates that the binding of the atoms making up the tubes is stronger than the binding among the tubes (this well-known effect is analogous to the transition-metal layered crystals, where the dispersion along the layer direction is much higher than that along the layer normal[30]). In the sulfur substances, the single state discussed above with a very high dispersion is found inside the gap.

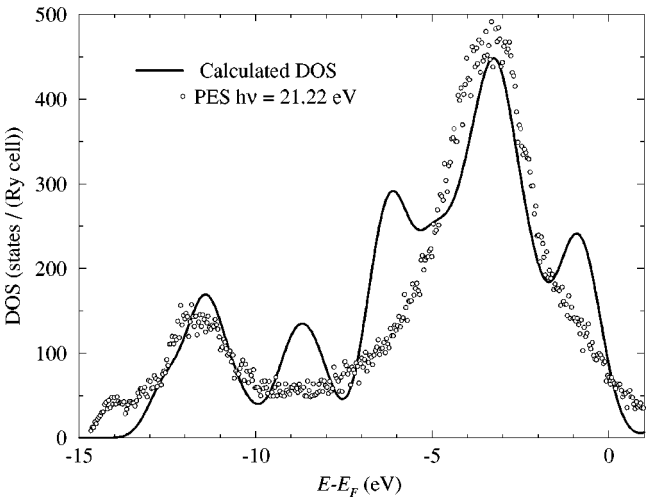

FIG. 6. Comparison of the photoemission spectrum for (Na;Se) (given in arbitrary units) and the density of states. The DOS has been calculated using the perturbational $\mathbf{k}\cdot\mathbf{p}$ method for 64 $\mathbf{k}$ points in the IBZ and has been convoluted with a Gaussian peak of 1 eV FWHM.

The strong Se character near the top of the valence band (see Sec. V A) gives a hint that the selenium of the pyramids is responsible for a large part of the photoconductivity. Electrons from there will be the first to be excited to the conduction band. Since the lowest conduction bands have strong contributions from orbitals of nearly all the atoms in the crystal no particular pathway for the conductivity can be deduced from their orbital composition. The two bands in the band structure marked by an asterisk in Fig. 7 are highly dispersive and prime candidates for the conduction of the electricity. At Γ the states are composed of selenium as well as the wall antimony and the oxygen orbitals, suggesting a zigzagging electron path between the selenium of the pyramids and the wall atoms.

The c axis dispersion of all bands has increased significantly with respect to the earlier muffin-tin calculations. However, similar bands are present also in the muffin-tin band structure, in particular the highly dispersive ones marked by the asterisk.

The valence band maximum appears on the top of the Brillouin zone with hardly any energetic difference among the states there. The highest energy is found at the A point, the conduction band minimum 1.3 eV above at the Γ point, at almost the same level with the ΓMK plane. The band structures of the three other substances are displayed in Fig. 8.

C. The dielectric function

The complex dielectric function has been calculated for all four crystals considered using the perturbational ap-

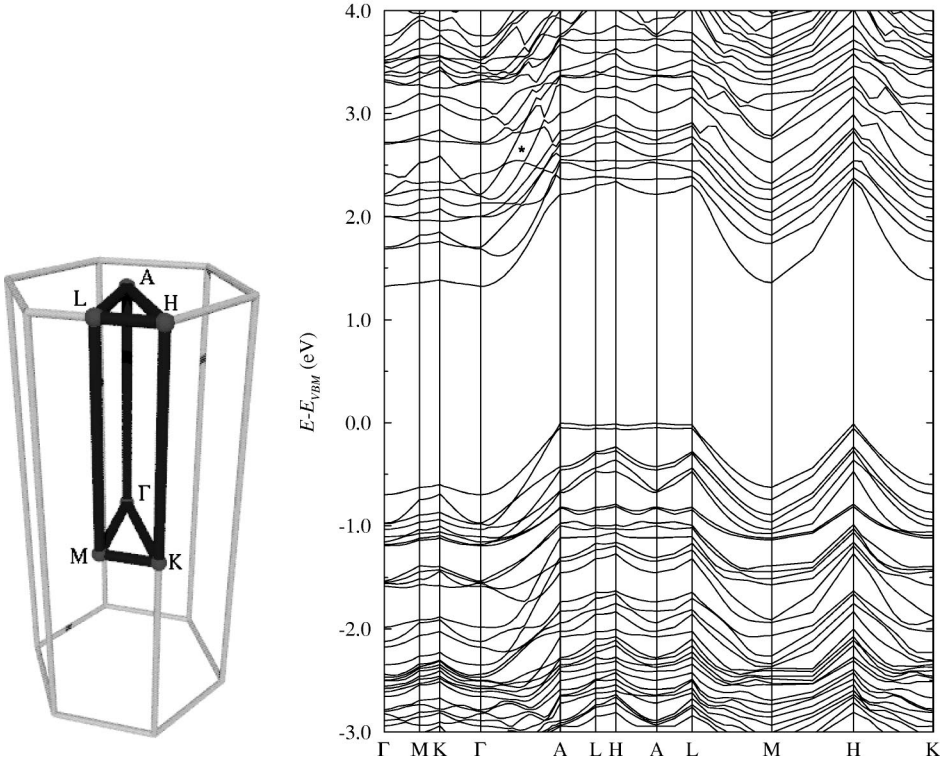

FIG. 7. Band structure of the (Na;Se) crystal in the hexagonal Brillouin zone, which is indicated on the left. An asterisk is used to denote the two dispersive bands noted in the text.

proach. The imaginary part is shown in Fig. 9 for **E** parallel to the crystal axis (the dependence of the function upon the polarization of the light is very small). Disregarding the (A;S) gap state, the sizes of the fundamental gaps are slightly larger than 2 eV, which is in excellent agreement with the experimental values for the gaps taken from transmission measurement.

The energy onset of optical absorption, as represented by the imaginary part of the dielectric function, is significantly smaller for (K;Se) than for the three other cetineites, which approximately have a common onset energy. (K;Se) differs in two respects from the other crystals: K 3p and Se 4s are strongly hybridized here and the optical properties are different. Experimentally, it is found that the substance crystallizes in a superstructure. While the experimental chemical trend given in Table II is clearly visible for the cetineites containing selenium, it is less distinguished for those containing sulfur. For (K;S), a maximum appears at a photon energy of about 0.8 eV which is due to transitions to the highly delocalized state in the gap. This peak is not visible in the experiment.

The comparison of the calculated absorption (see Fig. 10) with the measured transmission spectra shows that the chemical trend of the onsets of transmission in both theory and experiment agrees when cetineites of the same chalcogen and of the same alkali metal are compaired pairwise. We also have agreement in that the (Na;S) compound has the lowest onset and (K;Se) the highest. In the theoretical curves it is

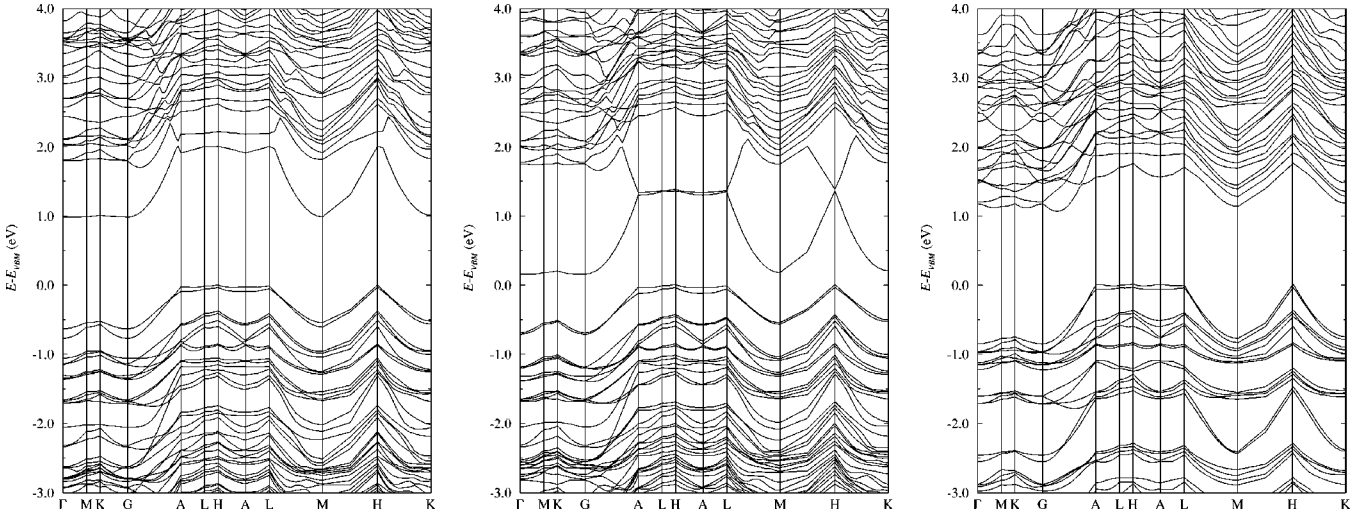

FIG. 8. Band structures of (Na;S) (left), (K;S) (center), and (K;Se) (right) calculated with the ELAPW AFC $\mathbf{k}\cdot\mathbf{p}$ method.

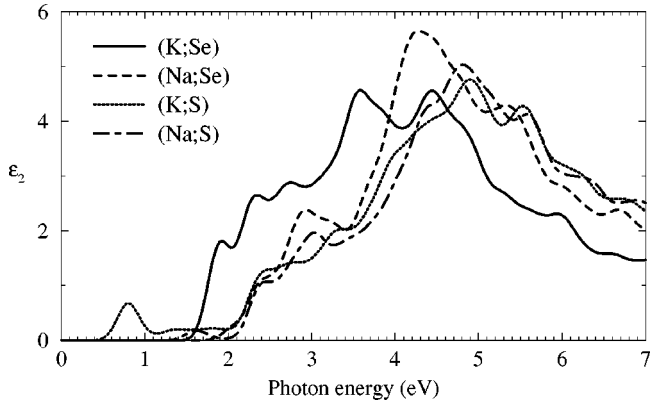

FIG. 9. The imaginary parts of the dielectric functions of the cetineites (K;Se), (Na;Se), (K;S), and (Na;S). The curves have been convoluted with a Gaussian of a FWHM of 0.25 eV. The electric field vector **E** is parallel to the crystal axis *c*.

difficult to determine, however, the relationship between (K;S) and (Na;Se).

D. Anisotropy of the electrical conductivity

Experimentally a strong anisotropy in the conductivity of cetineites has been measured[27,31] (see Table III). The conductivity has been measured in white light parallel and perpendicular to the *c* axis by applying silver contacts to (Na;Se) crystals as indicated in Fig. 11. Two of those crystals measured at room temperature yielded the results given in Table III, the typical variation with the sample preparation being visible in the difference of the results.

In (Na;Se) the conductivity along the tubes has been found to be by about a factor of 30 higher than perpendicular to it. For a theoretical comparison, the squared plasma frequencies $\omega^2_{p,\mu\mu}$ have been determined from the perturbational $\mathbf{k}\cdot\mathbf{p}$ results for 64 **k** points. The quantity $\omega^2_{p,\mu\mu}$ characterizes both the DOS and the averaged electron velocity at a given energy [see Eq. (1)]. While the conduction band DOS provides the final states for the photoexcitation process, the averaged velocity determines the electron mobility and thus the magnitude of the photocurrent, which is measured to yield the conductivity, in a given Cartesian direction μ. The $\omega^2_{p,\mu\mu}(E)$ curves are displayed in Fig. 12. The squared plasma frequencies are defined as

$$\omega^2_{p,\mu\mu}(E_F)=\frac{1}{\pi^2}\sum_{\lambda}\int dS_F\frac{v^2_{\lambda}(\mathbf{k})_{\mu}}{|\mathbf{v}_{\lambda}(\mathbf{k})|}, \tag{1}$$

where the integral is over the Fermi surface (below generalized to a **k** surface of constant energy), λ enumerates the energy bands, μ designates the real-space coordinates, and

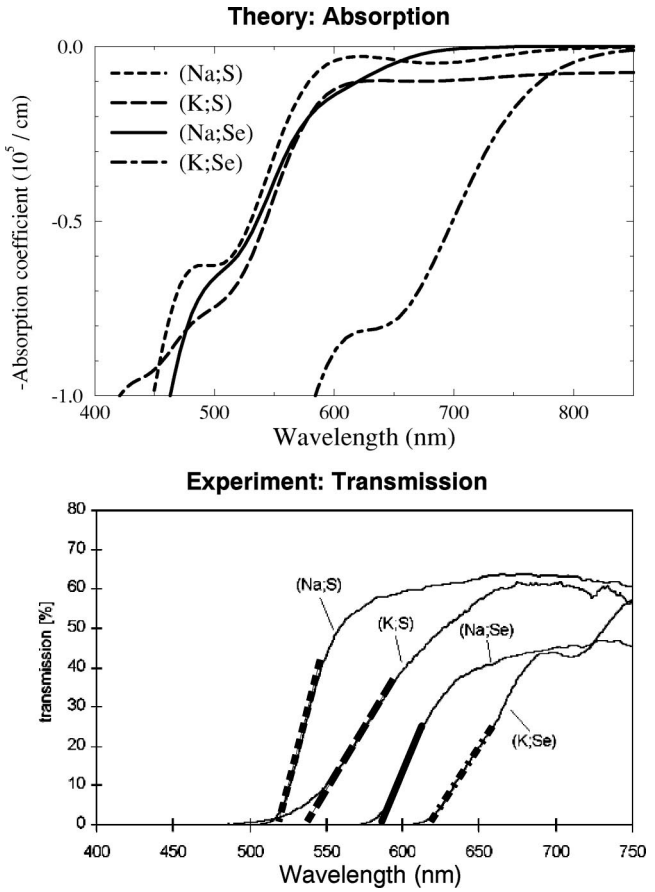

FIG. 10. The calculated absorption coefficient is compared with the measured transmission.

$v_{\lambda}(\mathbf{k})_{\mu}=\partial E_{\lambda}(\mathbf{k})/\partial k_{\mu}$. In a metal, the conductivity is proportional to the squared plasma frequency:

$$\sigma^{metal}_{\mu\mu}=\frac{\tau}{4\pi}\omega^2_{p,\mu\mu}(E_F). \tag{2}$$

The values $\omega^2_{p,\mu\mu}(E)$ shown in Fig. 12 can be interpreted for semiconductors as the conductivity electrons encounter when excited to states of a certain energy *E*, as in the photoconductivity experiments. Clearly, the conductivity is considerably higher along the *c* axis, that is, parallel to the tubes.

In a semiconductor, the conductivity tensor is given by an integral

$$\sigma^{nonmetal}_{\mu\mu}=\frac{\tau}{4\pi}\int dE\,\omega^2_{p,\mu\mu}(E)\left(-\frac{\partial f_0}{\partial E}\right), \tag{3}$$

where f_0 is the electron distribution function and τ the relaxation time. The Fermi distribution will not be strongly

TABLE III. The conductivity of two (Na;Se) crystals at room temperature parallel and perpendicular to the crystal axes (Refs. 10 and 27).

	Crystal 1	Crystal 2
Conductivity parallel $\sigma_{\parallel}$	5.4×10^{-7} S/m	6.8×10^{-7} S/m
Conductivity perpendicular $\sigma_{\perp}$	1.96×10^{-8} S/m	2.23×10^{-8} S/m
Factor $(\sigma_{\parallel}-\sigma_{\perp})/\sigma_{\perp}$	26.6	29.5

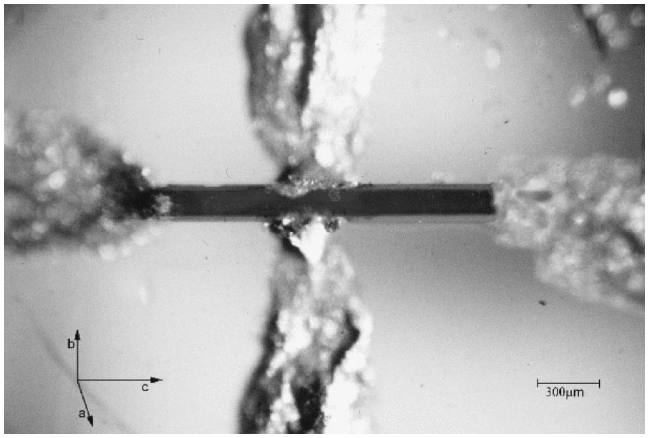

FIG. 11. A cetineite crystal contacted for measurement of the conductivity parallel and perpendicular to the crystal axis.

distorted by the temperature but the illumination will yield a nonzero distribution of carriers in the low conduction bands.

Since the function f_0 applies to both spatial directions equally, it is a good approximation to assume that the ratio of the plasma frequencies will translate to the conductivity. Clearly the conductivity is much higher in the direction parallel to c than perpendicular to it. For the first peak in the conduction band, ranging from 1.5 to 3 eV, at the maximum the ratio is $\omega_{p||}^2:\omega_{p\perp}^2=13:1$.

This result can be easily seen in the band structure (Fig. 7) where the stronger dispersion parallel to ΓA translates into the larger magnitudes of the derivatives parallel to this axis, which are integrated for the plasma frequencies. In the energy interval of the first conduction band peak a number of bands with a particularly high dispersion along ΓA can be observed, whereas around 3 eV the dispersion is reduced, which is reflected in the plasma frequencies. These results show that the order of magnitude of the anisotropy in the conductivity can be explained as a band structure effect.

The energy dependence of the plasma frequencies can also be used to extract the onset energies of the photoconductivity assuming that it will set in with the first extended maximum in the conduction band region. The mechanism supposed here is that valence band electrons are excited into conduction bands that show an appreciable conductivity as expressed by the plasma frequencies. We assume that the density of states near the valence band maximum is high enough to support a sufficient population of photoexcited

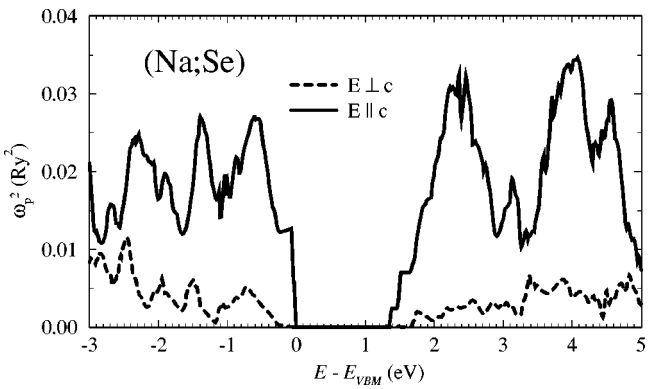

FIG. 12. The squared plasma frequencies for (Na;Se) calculated by the perturbational AFC ELAPW $\mathbf{k}\cdot\mathbf{p}$ technique.

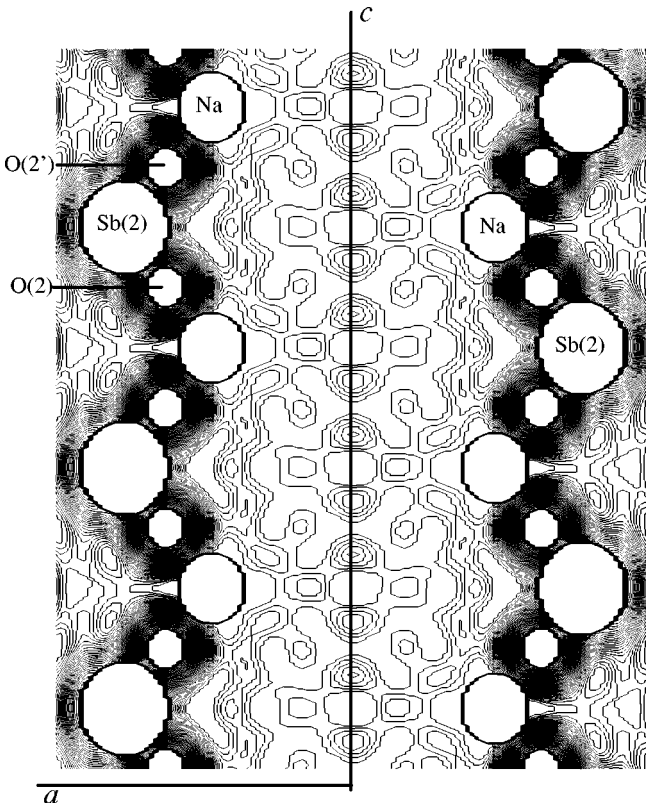

FIG. 13. The charge density of the cetineite (Na;Se) shown in a slice through the crystal that includes the tube axis (shown by the central line marked c) and is parallel to the axis a. Shown are three unit cells, i.e., the height of the graph is $3c$ and the width a.

carriers to yield the current measured in the photoconduction experiments. To estimate the lowest excitation energy for an experimentally significant photocurrent we look at the first maximum to make sure that the resulting current can really be measured and to exclude a contribution from the misleading structure of the delocalized states in the sulfur compounds. We expect those free-electron-like states not to be present in the samples due to guest atoms present in the tubes. Since the absolute size of the gaps is somewhat ambiguous due to LDA effects, our main aim here is to establish whether we can reproduce the trend of the gap sizes measured in the photoconduction experiments. The photoconductivity mechanism is different from that leading to the optical spectra where the transition probabilities between valence and conduction bands connected by the photon energy play a major role. When we look at the first extended maxima of the plasma frequency in the conduction band of the considered compounds (see Table II), we find that they follow the experimental gap sizes.

E. The electron density

The electronic density distribution in the cetineite (Na;Se) for the plane including the tube axis and being parallel to the crystal axis a is shown in Fig. 13 and a plane perpendicular to the c axis is shown in Fig. 14. The atomic spheres around the nuclei are left empty so as to make the atoms easier to identify. The charge density has been computed from the Γ point states, which is justified because of the very small Brillouin zone.

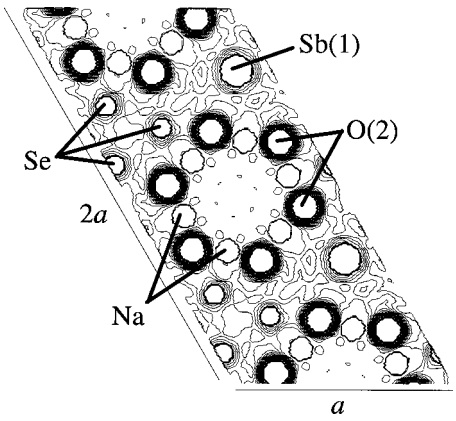

FIG. 14. The charge density of the cetineite (Na;Se) shown in a plane through the crystal perpendicular to the axis *c*. Two unit cells are shown. The plane is for $c=0.5$.

From the figures it is apparent that the tubes are nearly free of electronic density. The charge density between the atoms of the tube walls is quite high, indicating that the binding among the wall atoms is strong. Figure 14 shows that there is hardly any density surrounding the Na atom, although some of it will be covered by the large sphere. Nevertheless, in the third and fourth plane it is particularly visible that the Na atom is rather free of surrounding density in the opening in the wall made up of the oxygen atoms and Sb(2) and Sb(3). This confirms that in (Na;Se) the binding of the alkali metal to the pyramids, which is assumed to be responsible for holding the tubes together, is ionic in nature. This ionic binding has already been suggested by the DOS: the Na and Se states do not interact. Particularly the oxygen atoms are surrounded by a rather high electronic density. We have already mentioned the sizable contribution oxygen makes to the higher valence band where the states are made up of O $2p$ hybridized with Sb $5p$ or Se $4p$.

Since the density distribution does not include the excited states these figures cannot directly help interpreting the channels of conduction. However, the ground state density almost vanishing within the tubes, together with the nearly-free-electron-like excited density localized there, may indicate an unencumbered electron path when a voltage is applied to the ends of the tubes under light incidence or other excitational processes.

VI. CONCLUSIONS

The basic properties of the electronic structure of four cetineite crystals have been investigated. We have confirmed both experimentally and theoretically that the crystals are semiconductors. The size of the optical gaps has been understimated slightly in the theoretical results, which is not surprising for LDA calculations. In crystals containing sulfur there are delocalized states within the fundamental gap, and in the selenium compounds they are shifted to higher energies. The new AFC method significantly improves the values of the fundamental gaps compared to earlier muffin-tin calculations.

The strong anisotropy found in the conductivity of the crystals parallel and perpendicular to the *c* axis can be explained from the band structure. The dispersion along lines in reciprocal space parallel to ΓA is much stronger than that along those perpendicular to this line. This property of the band structure is visible in the theoretical conductivity, which is considered in the form of squared plasma frequencies. The calculations show that the conductivity along the axis is by about a factor of 10 stronger than that perpendicular to it. The measurements find an anisotropy factor of 30.

The atoms participating in the binding of the crystal have been found by determining the composition of the valence band density of states and the real-space charge density distribution. Particularly the oxygen atoms appear to be responsible for the stability of the tubes which are bound ionically to each other by the SbX_3 pyramids and the *A* atoms. Only in (K;Se) does a hybridization between the pyramids and the potassium appear at semicore energies. As a further singular property the optical gap is smaller by about 0.5 eV in this substance than in the others. (K;Se) is also the only cetineite that is known to crystallize in a superstructure. The effective hybridization of binding states may hint to a stronger bond of potassium to the host structure in (K;Se). It is thus less likely to interfere with guest molecules. This could explain why (K;Se) most easily can be filled with water molecules, for example, and why these molecules are most easily extracted from it, compared to other cetineites. The generally strong dispersion in the ΓA direction of all the cetineites suggests strong binding within the tubes but a rather weak interaction among them. This property is observed when the crystals are mechanically disintegrated.

The density of states of the top 15 eV of the valence band is in good agreement with an angle-integrated photoemission spectrum. Minor discrepancies may be due to experimental difficulties in the measurement of the crystals and the neglect of transition-matrix elements as well as water molecules inside the tubes in the calculations. Further investigations on these points are in progress.

The chemical trend found in the experiment for the optical gap width is in agreement with the theoretical results for the cetineites containing selenium. For the cetineites $(A;S)$ the gap size is nearly the same. The significant difference in the onset of optical absorption of (K;Se) from the other three cetineites may be connected to the above-mentioned hybridization of the potassium $3p$ and the selenium $4s$ orbitals. The squared plasma frequencies yield the onsets of the photoconductivity for the four crystals showing the same trend found in the experiment.

However, despite the wealth of information on the properties of cetineites gained so far a number of questions remain to be solved: What is the influence of the water or other guest molecules? What would be the result if not all the interstitial pyramid chains were oriented in the same direction? What is the exact nature of the delocalized state in the fundamental gap of the $(A;S)$ cetineites and how can we get experimental evidence on it? Work on these questions is ongoing.

ACKNOWLEDGMENTS

This work was supported by the Deutsche Forschungsgemeinschaft under Contracts Nos. SI 609/2-1 and SCHA 360/14-1.

[1] C. Sabelli and G. Vezzalini, N. Jb. Miner. Mh. **9**, 419 (1987).
[2] J. V. Smith, Chem. Rev. **88**, 149 (1988); S. L. Suib, *ibid.* **93**, 803 (1993).
[3] G. A. Ozin, Adv. Mater. **4**, 612 (1992).
[4] U. Vietze, O. Krauß, F. Laeri, G. Ihlein, F. Schüth, B. Limburg, and M. Abraham, Phys. Rev. Lett. **81**, 4628 (1998).
[5] M. Reed, Sci. Am. **268** (1), 98 (1993).
[6] G. Schön and U. Simon, Colloid Polym. Sci. **273**, 101 (1995); **273**, 202 (1995).
[7] X. Wang, F. Liebau, Eur. J. Solid State Inorg. Chem. **35**, 27 (1998); X. Wang and F. Liebau, Z. Kristallogr. **214**, 820 (1999).
[8] U. Simon, F. Schüth, S. Schunk, F. Liebau, and X. Wang, Angew. Chem. Int. Ed. Engl. **36**, 1121 (1997).
[9] U. Simon, J. Jockel, F. Starrost, E. E. Krasovskii, and W. Schattke, Nanostruct. Mater. **12**, 447 (1999).
[10] U. Simon, J. Jockel, F. Starrost, E. E. Krasovskii, W. Schattke, B. Marler, S. Schunk, M. Wark, and H. Wellmann, Stud. Surf. Sci. Catal. (to be published).
[11] F. Starrost, E. E. Krasovskii, W. Schattke, X. Wang, F. Liebau, J. Jockel, and U. Simon, Z. Kristallog. Suppl. **13**, 90 (1998).
[12] F. Starrost, E. E. Krasovskii, W. Schattke, J. Jockel, U. Simon, X. Wang, and F. Liebau, Phys. Rev. Lett. **80**, 3316 (1998).
[13] E. E. Krasovskii, F. Starrost, and W. Schattke, Phys. Rev. B **59**, 10 504 (1999).
[14] C. Sabelli, I. Nakai, and S. Katsura, Am. Mineral. **73**, 398 (1988).
[15] H. A. Graf and H. Schäfer, Z. Anorg. Allg. Chem. **414**, 220 (1975).
[16] F. Liebau and X. Wang, *Annual Meeting Abstract Book* (American Crystallographic Association, Pittsburgh, 1992), p. 128.
[17] X. Wang, Z. Kristallogr. **210**, 693 (1995).
[18] X. Wang, *8. Deutsche Zeolith-Tagung* (DECHEMA e. V., Berlin, 1996).
[19] J. Jockel, Master's thesis, Fachbereich Chemie der Universität GH Essen, 1996.
[20] A. Thess, R. Lee, P. Nikolaev, H. Dai, P. Petit, J. Robert, C. Xu, Y. Hee Lee, S. Gon Kim, A. G. Rinzler, D. T. Colbert, G. E. Scuseria, D. Tománek, J. E. Fisher, and R. E. Smalley, Science **273**, 483 (1996).
[21] E. E. Krasovskii, Phys. Rev. B **56**, 12 866 (1997).
[22] E. E. Krasovskii, A. N. Yaresko, and V. N. Antonov, J. Electron Spectrosc. Relat. Phenom. **68**, 157 (1994).
[23] E. Wimmer, H. Krakauer, M. Weinert, and A. J. Freeman, Phys. Rev. B **24**, 864 (1981).
[24] X. Wang, Ph.D. thesis, Kiel University, 1993.
[25] E. E. Krasovskii, O. V. Krasovska, and W. Schattke, J. Electron Spectrosc. Relat. Phenom. **83**, 121 (1997).
[26] W. Wolf, G. Bihlmayer, and S. Blügel, Phys. Rev. B **55**, 6918 (1997).
[27] U. Simon, Habilitation thesis, Universität GH Essen, 1998.
[28] X. Blase, A. Rubio, S. G. Louie, and M. L. Cohen, Europhys. Lett. **28**, 335 (1994).
[29] F. Starrost, E. E. Krasovskii, and W. Schattke, Verhandl. DPG (VI) **33**, 741 (1998).
[30] A. Leventi-Peetz, E. E. Krasovskii, and W. Schattke, Phys. Rev. B **51**, 17 965 (1995).
[31] U. Simon, J. Jockel, F. Starrost, E. E. Krasovskii, and W. Schattke (unpublished).